McCoy, T. M., Brown, P., Eastoe, J., & Tabor, R. F. (2015). Noncovalent magnetic control and reversible recovery of graphene oxide using iron oxide and magnetic surfactants. *ACS Applied Materials and Interfaces*, *7*(3), 2124-2133. https://doi.org/10.1021/am508565d

Magnetic control and reversible recovery of graphene oxide using hematite and magnetic surfactants

Thomas M. McCoy,[†] Paul Brown,[‡] Julian Eastoe,[¶] and Rico F. Tabor[*,†]

School of Chemistry, Monash University, Clayton, VIC 3800, Australia, Department of Chemical Engineering, Massachusetts Institute of Technology, Cambridge MA, USA, and School of Chemistry, University of Bristol, BS8 1TS, UK

E-mail: rico.tabor@monash.edu

Phone: +61 3 9905 4558. Fax: +61 3 9905 4597

Abstract

The unique charging properties of graphene oxide (GO) are exploited in the preparation of a range of non-covalent magnetic GO materials, using microparticles, nanoparticles and magnetic surfactants. Adsorption and desorption is controlled by modification of pH within a narrow window of < 2 pH units. The benefit conferred by using charge-based adsorption is that the process is reversible, and the GO can be captured and separated from the magnetic nanomaterial, such that both components can be recycled. Hematite microparticles form a loosely flocculated gel network with GO, which is demonstrated to undergo magnetic compressional dewatering in the presence of an external magnetic field. For composites formed from GO and hematite nanoparticles, it

[*]To whom correspondence should be addressed
[†]Monash University
[‡]MIT
[¶]University of Bristol

is found that low hematite:GO mass ratios ($< 5:1$) favour flocculation of GO, whereas higher ratios ($> 5:1$) cause overcharging of the surfaces resulting in restabilization. The effectiveness of the GO adsorption and magnetic capture process is demonstrated by separating traditionally difficult-to-recover gold nanoparticles ($d \approx 10$ nm) from water. The fully recyclable nature of the assembly and capture process, combined with the vast adsorption capacity of GO, presents obvious and appealing advantages for applications in decontamination and water treatment.

Keywords: Graphene oxide; adsorption; hematite; magnetic nanomaterials; magnetic surfactants.

Introduction

Graphene oxide (GO) has attracted huge research momentum in recent years due to its potential in a vast array of applications including optics,[1] stabilization of interfaces[2,3] and more recently, water treatment.[4] GO readily disperses in water to form stable colloidal dispersions, facilitating its deployment in aqueous systems.[5] This effect stems from the low acidity constant of carboxyl groups at the periphery of GO sheets ($\mathrm{p}K_a = 4.3$), meaning they readily dissociate into carboxylate anions.[6] Therefore, GO maintains a negative surface charge down to very low values of pH (< 1) retaining charge-based stability across a wide pH range.[7] These surface properties, along with the vast surface area to mass ratio provided by the sheets explain to a large extent why investigations into the use of GO as an adsorbent material for removal of toxins from aquatic environments is becoming increasingly prevalent.

Previous studies have shown that GO is a suitable material for purifying water of many

types of pollutants, from antibiotics[8] to heavy metals.[9] Typical adsorption capacities of GO of *ca* 100 mg/g for heavy metal ions[9,10] are approaching those seen for the zeolites typically used,[11] with the advantage that GO is readily and cheaply prepared from abundant natural graphite deposits. These discoveries have inspired the development of a wide variety of graphene and graphene oxide composite materials that have shown great potential for many environmental applications concerning pollution.[12] Certain composites have been ideally formulated and proven to be effective in the adsorption of gases,[13,14] while others are specialized for removing certain compounds from water such as dye molecules.[15]

However, for the use of GO in the capture of pollutants to be feasible, the material would need to be recovered following sorption. This realization has lead to the production of GO composites containing magneto-responsive components, providing a simple method for removing the material from solution after it has been deployed. Magnetic composites incorporating GO and reduced GO have been successfully implemented in the removal of many toxic metal elements from aqueous systems including arsenic,[16,17] cadmium,[18] selenium[19] and mercury.[20] In each of these accounts, the magnetic nanoparticles are introduced to the GO through synthetic pathways that *covalently* bind the particles to the surfaces of the sheets.

The drawback to using GO composite materials is that their production often involves complex, high energy and multi-step procedures that permanently change the structural makeup of the GO. In addition, they have a comparatively narrow range of uses. Therefore, in essence, the utilization of pure, 'virgin' GO as an adsorbent for water decontamination would be ideal. Aside from being difficult to remove from solution, GO also possesses in vivo, toxic characteristics associated with its oxygenated functional groups.[21] Hence, viable methods for recovering GO from solution must be developed for its use in large-scale industry to be plausible.

Hematite (α-Fe_2O_3) is a magnetic compound that naturally occurs in large abundance.[22] Its surface chemistry is dependent on pH in aqueous media, with an isoelectric point (IEP) of 7-8.[23,24] Therefore, in a solution at pH values below its IEP, the hematite particles would be expected to experience strong, charge-based attractions with GO sheets, arising from the opposing surface charges. Similarly, the magnetic ionic liquid surfactants: 1-methyl-3-butylimidazolium tetrachloroferrate and dodecyltrimethylammonium trichloromonobromoferrate, abbreviated henceforth to 'mim' and 'DTA' respectively, should interact with the GO in a similar manner.[25]

This study investigates and demonstrates how surface charge can be manipulated to control the adsorption of magnetic substances onto GO, and facilitate its removal from water. Our methods utilise cheap and readily processed materials that circumvent the need to perform difficult and lengthy syntheses of GO nanocomposites, and are low energy alternatives to centrifugation and polymer flocculation. In addition, capture of GO *via* this route is fully reversible as the GO can be redispersed into the solution by readjusting the system pH. Because the GO is unaltered by this process, there is no compromise to its original properties following adsorption, thus the GO and magnetic material can be reused. The experimental concept is shown schematically in Fig. 1a.

Results & discussion

Characterization of materials

Graphene oxide (GO) was synthesized from graphite particles using an improved Hummer's method.[27] The shape and size of the resulting particles were then characterized by atomic force microscopy (AFM) (see Supporting Information) and were found to be almost entirely

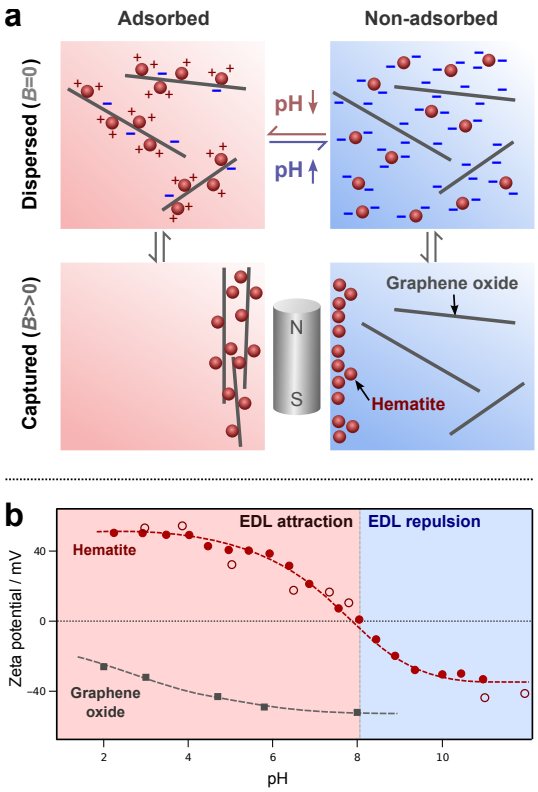

Figure 1: (a) Conceptual shematic of the experiment: pH adjustment is used to effect charge attraction or repulsion between the GO sheets and hematite particles. A magnetic field can be used to separate the hematite from solution or dispersion. (b) Zeta potentials of graphene oxide and hematite nanoparticles, demonstrating the pH ranges at which electrical double-layer (EDL) attraction or repulsion would be expected. Data for hematite are from Palomino and Stoll[24] (solid symbols) or measured in this work using hematite nanoparticles (open symbols) and for GO are from Chen *et al.*[26]

1 nm in thickness, indicative of monolayer GO.[3,28,29] The lateral dimensions were typically several micrometres, with the average flake sizes characterized previously by dynamic light scattering.[30]

Optical properties were characterized by UV-visible spectrophotometry (see Supporting Information), which was also used to quantify GO concentrations throughout, having been initially calibrated gravimetrically. The spectra display the distinctive features expected for GO: a distinct absorption maximum at approximately 230 nm corresponding to $\pi \rightarrow \pi^*$ transitions, and a shoulder at around 300 nm, believed to be $n \rightarrow \pi^*$ transitions.[31]

~~Graphene oxide and hematite microparticle systems~~

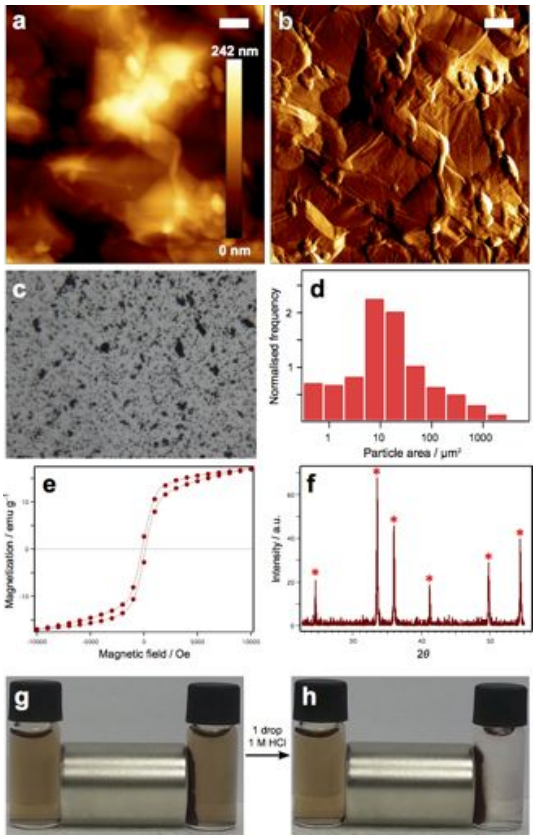

Figure 2: GO adsorption and recovery using hematite microparticles: (a) AC mode AFM height image showing GO adsorbed onto hematite microparticles. (b) The corresponding AFM amplitude image highlighting edge features. In (a) and (b), the white scale bars represent 200 nm. (c) Micrograph of hematite microparticles at ×100 magnification. The horizontal dimension of the image is 120 μm. (d) A histogram showing the size distribution (projected area) of the particles in (c). (e) Hysteresis loop showing magnetization of the hematite microparticles as a function of applied magnetic field. (f) Powder X-ray diffraction spectrum of the microparticles, with expected positions of peaks for hematite shown with asterisks. (g & h) The effect of an external magnetic field on GO (0.2 mg/mL) without (left vials) and with (right vials) added hematite microparticles (0.05 g) at high (e) and low (f) pH, demonstrating the separation of hematite from GO in the non-adsorbed state and capture of GO-hematite complex when adsorption occurs at low pH.

Hematite (α-Fe_2O_3 microparticles were characterised using atomic force and optical microscopies, superconducting quantum interference device (SQUID) magnetometry and powder X-ray

diffraction (PXRD), demonstrating their morphology, size, magnetization and crystal structure respectively (Fig. 2). To investigate the magnetic response of hematite, a full magnetic hysteresis curve was produced. The microparticles exhibited fairly weak ferromagnetism at room temperature due to the Dzyaloshinsky-Moriya mechanism,[32,33] with field-dependent magnetization around 16 emu g^{-1}. This is much larger than might be expected, but is not suprising for a precipitated material with small crystal domain sizes.[34] No saturation was observed in the range studied (-10,000 Oe < H > 10,000 Oe). The coercivity approached 250 Oe.

Graphene oxide and hematite microparticle systems

From the large difference in isoelectric points for GO (pH $\approx$ 0) and hematite (pH $\approx$ 7), a wide window exists in which the two materials exhibit opposite surface charges (Fig. 1b) and thus could be expected to experience attraction due to their electrical double-layers. Previous work at gold-water interfaces has indicated that the approach of assembly *via* charge attraction works well for GO,[30] as have various layer-by-layer assembly studies.[26,35–37]

To assess the feasibility of magnetically extracting the GO using charge-assembled magnetic materials, mixtures of GO and hematite microparticles were explored as a function of pH (Fig. 2). AFM imaging of GO on the particle surfaces (Fig. 2a,b) indicated that it adsorbs conformally (*i.e.* lying flat over the particle surfaces). The particles used had an average radius *ca.* 2 μm, calculated from their projected area (Fig. 2c,d). These hematite particles were only kinetically stable in water, and settled over time.

In order to exemplify the charge-mediated adsorption of GO onto the hematite particles, Fig. 2e and f show the same set of vials at different pH conditions. In all cases, the two vials both contain GO (0.2 mg/mL), but in each frame the right hand vial also contains 50 mg of

hematite microparticles. At high pH (Fig. ~~2e~~2g) no change in the colour of the solution is seen when hematite was added and the sample placed by a magnet, indicating that all of the GO remained dispersed while the hematite is captured by the magnet. However, once the solution had been marginally acidified (pH < 5), the GO and hematite co-flocculated and were both captured by the magnet (Fig. ~~2f~~2h). This serves as a clear indication as to the importance of pH and charge in controlling the surface chemistry in these systems. Although iron oxides become more soluble at low pH, Jang *et al.* showed that hematite dissolution is vanishingly slow at the pH values dealt with here.[38]

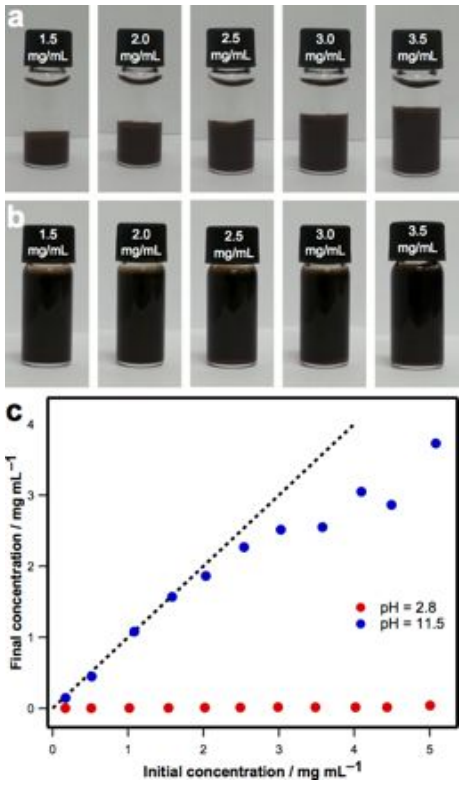

Figure 3: Flocculation of GO using hematite microparticles: (a) Samples containing 20 mg of hematite with varying concentrations of aqueous GO dispersion at pH 2.8. (b) Equivalent samples to those in (a) but at pH 11.5. (c) UV-visible spectrophotometry data showing the concentration of GO remaining in the supernatant layer at high and low pH as a function of initial GO concentration. The dashed, black line shows a y=x trend for comparison (*i.e.* the limit of no adsorption).

To explore this effect quantitatively, a range of pH and concentration ratios were explored.

At low pH the GO and hematite coprecipitate to form a magnetically responsive 'network' that settles out quickly, leaving clear water as the supernatant (Fig. 3a). It is notable that this co-flocculated material appears to be a gelled particle network, as the volume occupied is many times greater than the dry volume occupied by the constituent hematite and GO. The higher the concentration of GO, the greater the volume of the 'network'. Conversely, at high pH, no precipitation of the GO was seen, and it remained dispersed in the water while the hematite settled (Fig. 3b).

This effect is readily explained by strong charge attraction between the positive hematite surfaces and the negative periphery of the GO sheets, due to the dissociated carboxylate groups. We therefore posit a structure for this network whereby GO sheets link hematite particles, acting as a bridging flocculant, in much the same way that many polyelectrolytes are used as particle flocculants.[39]

At pH 11.5, the GO and hematite are both strongly negatively charged and hence experience a mutual repulsive electrical double-layer force. At pH 2.8, the GO maintains its negative surface charge, however the hematite particles are strongly positively charged from protonation of their surface oxide groups. It can be seen that effectively all of the GO has been removed from the bulk solution in the low pH samples, whilst for the high pH samples, the majority of the GO is still present (Fig. 3c). Some removal appears to have occurred for the higher concentrations of GO at high pH, though this may be due to a self-salting effect where the high volume fraction causes overlap of the electrical double-layers of the GO sheets, resulting in a locally increased counterion concentration that acts to 'salt out' the sheets *via* charge screening.[40–43]

Exploring the effects of pH indicates a relatively narrow window in which the transition

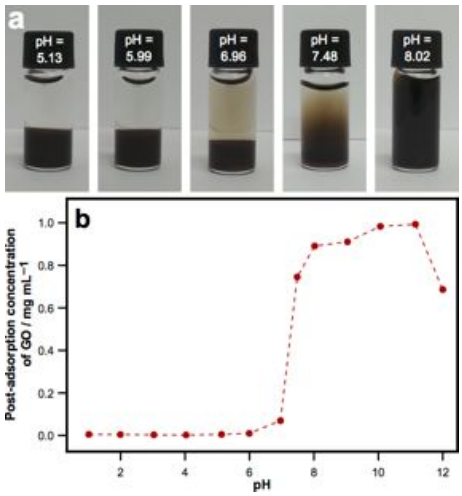

Figure 4: The effect of pH on flocculation of GO with hematite: (a) Samples containing GO at 1.5 mg/mL with 20 mg of hematite microparticles present at different pH values. (b) UV-visible spectrophotometry data showing the concentration of GO remaining in the supernatant layer as a function of pH for the fixed starting concentrations specified in (a).

between complete flocculation and full dispersion is seen (Fig. 4). The results show that at pH values of 6 and below, close to pure water can be retrieved. At pH 6.96, marginally below the isoelectric point of hematite, the majority of the GO had adsorbed, leaving a low concentration in dispersion and a slightly smaller GO/hematite network. Just above the isoelectric point of hematite (pH = 7.48), some settling and adsorption is apparent, however most of the GO remains dispersed. At pH values of 8 and above, the GO stays almost fully dispersed. The apparent decrease in dispersed GO seen at pH 12.00 is most likely a result of the GO starting to become chemically reduced, which is known to occur at high pH.[30,44]

Graphene oxide and hematite nanoparticle systems

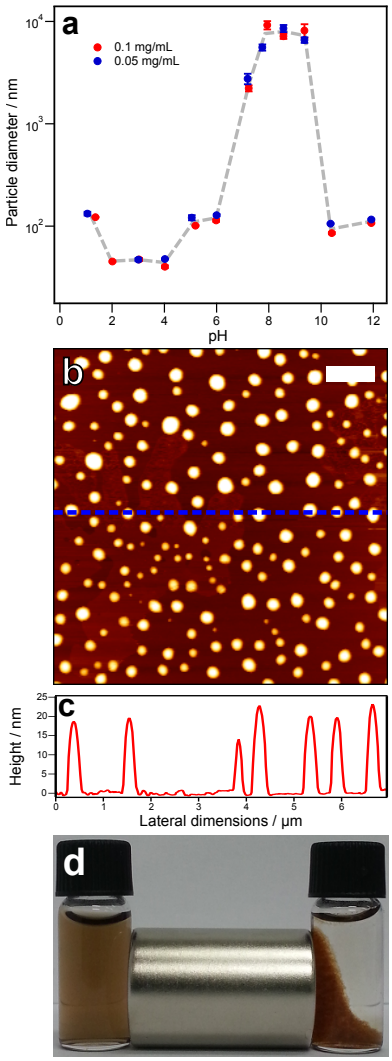

Figure 5: (a) Apparent hydrodynamic diameters of synthesised hematite nanoparticles as a function of pH as determined using dynamic light scattering (DLS). Error bars correspond to the standard error for each point and the dashed line is a guide to the eye. (b) AFM height image of hematite nanoparticles dried onto mica. The white scale bar represents 1 μm, and the dashed, blue line shows the position of a cross-sectional height profile that is presented in (c). (d) The magnetic extraction of GO in water using hematite nanoparticles. Both vials contain 0.2 mg/mL of GO, however the right-hand vial also includes a 0.2 mg/mL concentration of nanoparticles.

Although microparticles are appealing for reversible capture and dispersion of GO due to the large magnetic force they experience, they suffer from the problem of settling, which means that energy is required to effectively disperse them for capture of GO. At small scales and in

stirred, flowing or otherwise agitated systems (such as waste-water settling tanks, pipe flow, *etc.*) this does not represent a significant problem. However, deployment at larger scales requires a magnetic capture agent that is colloidally stable - that is, a material that will not settle over time but will remain dispersed due to Brownian collisions with solvent molecules.

Our solution was to explore the deployment of small, hematite nanoparticles that form thermodynamically stable dispersions. These nanoparticles were synthesized from iron (II) sulphate heptahydrate using the procedure described by Chen *et al.*[45] Dynamic light scattering (DLS) results indicate that the nanoparticles are most stable at low pH (2-4) where their surface charge is strongly positive. Their apparent effective diameter at this point is *ca.* 40 nm, whereas the particles readily attract one another and form larger flocs at pH 7 - 9 (Fig. 5a), close to the isoelectric point of the particles where the surface potential drops below the 30 mV required for colloidal stability. AFM imaging indicated that the particles were mostly below 20 nm in size, with surprisingly low polydispersity (Fig. 5b,c). A mixture of hematite nanoparticles with aqueous GO dispersion at pH 3 resulted in a flocculated material that was highly responsive to an external magnet (Fig. 5d).

To confirm specific adsorption of the hematite nanoparticles to the GO sheets, the GO-nanoparticle composite material formed at pH 3 was imaged using AFM (Fig. 6a). It is clear that the hematite nanoparticles show high and specific affinity for the GO, forming large clusters on the surfaces of the sheets. This suggests that again, electrical double-layer interactions are the driving force behind the adsorption and flocculation processes, as strikingly few nanoparticles were seen on the mica substrate. Moreover, it is clear from Figure 6b that there is a highly specific pH range within which optimal interaction between the nanoparticles and GO occurs, with no adsorption being evident in the high pH sample. This is again in line with expectation from the surface charging behaviour of hematite and GO, and echoes the characteristics of the hematite microparticle dispersions.

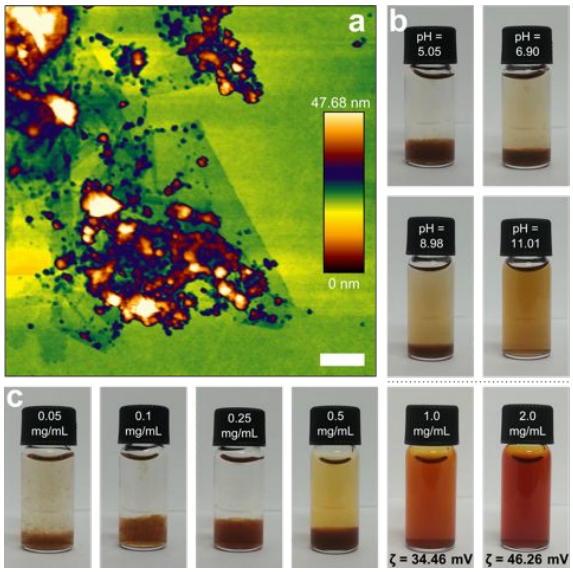

Figure 6: (a) AFM height image of hematite nanoparticles adsorbed onto sheets of graphene oxide at pH 3 and dried onto mica. The scale bar represents 200 nm. (b) Samples containing 0.15 mg/mL of aqueous GO and 0.15 mg/mL hematite nanoparticles at different pH values. (c) Samples containing 0.1 mg/mL of GO in water (pH 3) and increasing concentrations of hematite nanoparticles.

Despite the significant difference in lateral dimensions between the hematite nanoparticles and the microparticles studied above, the mechanism of co-flocculation is likely similar, whereby the nanoparticles act to bridge the GO sheets, causing a 3D network to form. The number of effective cross-links between sheets would therefore be related to the ratio of nanoparticles to GO, with higher nanoparticle loadings favouring a denser network structure due to a larger number of 'linkages'. This appears to be realised (Fig. 6c) where increasing nanoparticle loading for the same amount of GO results in a smaller, denser flocculated layer. By nanoparticle:GO ratios of >3:1, free (unflocculated) nanoparticles are evident in the supernatant above the flocculated GO.

It is found therefore that an equal mass ratio of hematite nanoparticles to GO is ideal for recovery. However, a particularly interesting effect occurs at higher nanoparticle loadings,

whereby re-stabilization of the GO was observed. Dispersions thus formed were indefinitely stable, indicating a surface potential above the 30 mV generally required for colloidal stability. We posit that this effect occurs due to overcharging of the particle surfaces, whereby the hematite nanoparticles act as a dispersant for the GO, increasing the surface potential of the composite material to large, positive values. A similar effect has been seen whereby small, highly charged nanoparticles stabilise larger colloids with low, opposite surface charges by adsorption,[46] with the effect explained as a balance of van der Waals attractions and electrical double-layer effects. Similarly, the 'supercharging' of anionic silica by adsorption of anionic surfactants has been noted, suggested to be entropic in origin.[47] The concentration-dependent flocculation/redispersion effects for nanoparticle adsorption on GO seen here are to our knowledge the first such example for such a nanomaterial, and thus may be advantageous in designed systems for bulk solution deployment of GO.

Graphene oxide and magnetic surfactant systems

There has been a recent surge of interest surrounding the use of magnetic surfactants as stabilizers, due to their ability to form micelles, microemulsions and (macro) emulsion droplets as soft colloids with magnetic response.[48,49] They have also been employed in the field-induced control of biomacromolecules[50] and more recently, silica particles.[51] However as yet, their application for the magnetic recovery of nanomaterials remains unexplored. We investigate the potential of two such surfactants, 1-decyl-3-methylimidazolium tetrachloroferrate (mim) and dodecyltrimethylammonium trichloromonobromoferrate (DTA) as molecular alternatives to the microparticle and nanoparticle systems examined above. Adsorption experiments were carried out at pH 5.5 to ensure that the GO had a significant negative surface charge.

Interestingly, the behaviour of the magnetic surfactant/GO systems is similar to the hematite systems (Fig. 7a,b), and the surfactant appears to serve two roles: firstly as a magnetic material for field-induced recovery of the GO, but also as a flocculant. The surfactants were

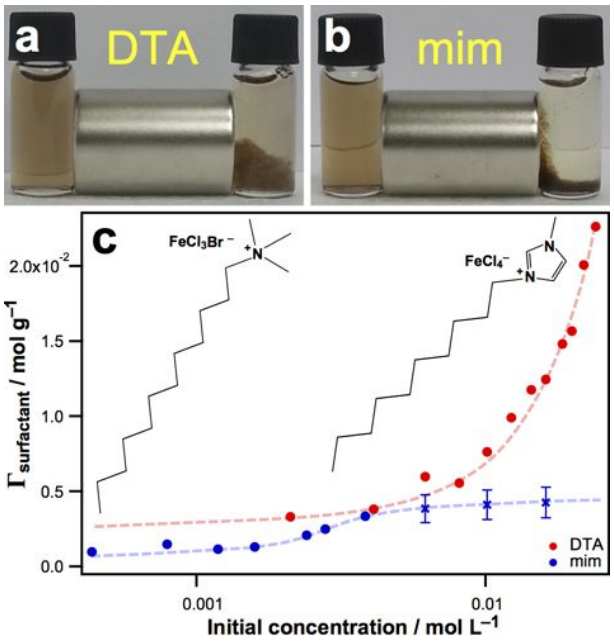

Figure 7: (a & b) Magnetic response of magnetic surfactant-GO systems: all samples contain 0.2 mg/mL GO in water, but only the right-hand vials contain additionally 1 mM surfactant, of which the corresponding molecular structure is shown directly beneath the vials. (c) Adsorption isotherms for each surfactant on GO. Due to difficulties encountered in obtaining spectra for the higher concentrations of mim, approximate points (marked with crosses) have been added to demonstrate the approximate adsorption saturation concentration. The dashed trendlines have been added as guides to the eye.

chosen for their positively charged head-groups, as these should experience a strong electrostatic attraction to the dissociated carboxylate groups on GO. To explore these characterstics further, adsorption isotherms for each surfactant on GO were constructed (Fig. 7c). It is seen that mim has a relatively low affinity for GO, adsorbing at less than 0.5 moles of surfactant per gram of GO even at high surfactant loadings. DTA on the other hand adsorbs with moderate affinity at high surfactant concentrations, though we were unable to observe adsorption saturation (asymptotic flattening of the isotherm) due to the experimental uncertainties associated with measuring small changes in absorbance at large concentrations.

The large difference in affinity aids interpretation of the magnetic response of the two systems (Fig. 7a,b). The DTA-GO system shows significant flocculation, forming a loosely-

aggregated GO matrix, which is moderately attracted to the magnet. Conversely, the mim-GO system forms a much denser flocculated material of which only a small amount responds to the magnet. Thus it is clear that the more strongly adsorbed DTA surfactant is the more effective of the two for magnetic recovery of GO. We theorise that there are two possible reasons for the flocculation behaviour encountered for the surfactants here: a) the surfactant adsorbs strongly to the anionic carboxylate groups around the GO periphery, thus neutralising the charge and causing colloidal instability; or b) the GO sheets become coated with a large amount of surfactant and are therefore rendered hydrophobic and attract one another. Given the high concentrations of surfactant required for significant adsorption, the second explanation seems much more likely. Similar flocculation behaviour is seen for GO when reduction due to increased pH occurs,[30] which also supports this hypothesis.

As it is the counterion that is paramagnetic, rather than the surfactant ion itself, this raises an important question about the nature of the adsorption and magnetic response. Clearly the fractional level of counterion dissociation is a key parameter, and this was previously determined using small-angle neutron scattering as 0.73 and 0.81 for mim and DTA respectively.[25] These values are high compared to the same surfactant ions with 'conventional' bromide or chloride counterions,[25] indicating an increased hydrophilicity of the iron-containing, magnetic counterions. Thus it is suspected that bound surfactants contribute to the magnetic response of the surfactant-GO materials in two ways. The first is that undissociated, bound surfactants (adsorbed *via* hydrophobic interactions with the GO sheets or polar interactions) will directly respond to the magnetic field. The second is that dissociated, bound surfactant ions still retain their counterions in a diffuse layer near the surfactant-GO interface, and that by magnetic movement of the dissociated counterions, the surfactant-GO complex is osmotically 'dragged' with them. The relative contributions of these two effects would depend on binding strength and concentration, and modelling studies are underway to understand this further.

Magnetic compression and dewatering of GO

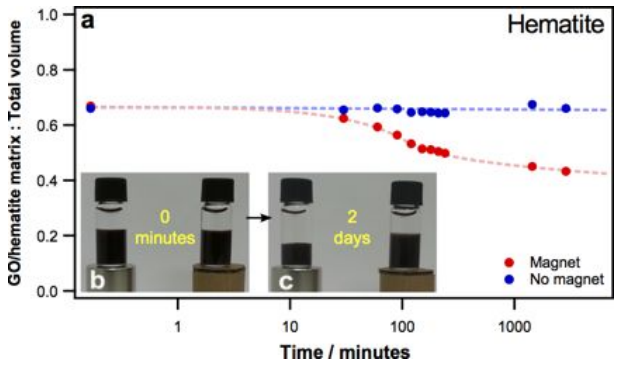

Figure 8: Magnetic compression of GO-hematite materials: (a) The change in volume of a GO-hematite microparticle matrix as a function of time when one is subjected to a magnetic field and the other is not. Measuring began after the initial settling due to gravitational forces had ceased. (b & c) Images of the two identical samples when first placed on the magnet/cardboard magnet (b), and two days later (c).

For each of the magnetic materials employed, pH-dependent GO flocculation was observed, and so it is pertinent to more systematically study the magnetic response of the co-flocculated materials generated. In particular, the magnetic compressibility of the flocculated material was explored by placing the materials on a strong permanent magnet and recording the volume of the flocculated network as a function of time (Fig. 8).

For the case of hematite microparticles, the volume of the GO/hematite matrix was almost halved over a two day period (Fig. 8a-c), indicating significant compression and dewatering. However, when the same test was performed on systems containing hematite nanoparticles or the magnetic surfactants, effectively no compaction occurred (see Supporting Information). It is possible that in the cases with the nanoparticles and surfactant molecules, the matrix is denser or more strongly bonded, and therefore unable to compact further regardless of the magnet being present. However, an examination of the energy experienced per particle due to the magnetic field is also illuminating: a 2 μm radius hematite particle, typical of the microparticle material, would experience an energy due to the magnet of around 7×10^{-15} J

(assuming a typical magnetization of 200 A/m for finely divided hematite[52]). A 20 nm radius particle with the same characteristics however would gain an energy of only 7×10^{-21} J, around the same magnitude at thermal energy, $k_{\mathrm{B}}T$ at 298 K, 4.1×10^{-21} J. It is difficult to precisely estimate the energy for the surfactant system, but it is expected to be of a similar magnitude *per unit mass* as hematite, given the susceptibilities of the surfactants themselves.[25]

It should also be noted that the mass ratio for magnetic surfactant and nanoparticle experiments (around 1:1 magnetic material:GO) was significantly less than for the microparticle case (2.6:1 magnetic material:GO), also contributing to the increased effectiveness of microparticles. This does however indicate that by transitioning to nanomaterials where surface area-to-volume ratios are significantly higher, lower loadings can be used to capture GO from dispersion.

It is clear that the hematite microparticles are able to exert a significantly larger force on the GO matrix, and although the nanoparticles and surfactants apply sufficient force in a magnetic field to act against Brownian motion to enable collection of the material with a magnet, they cannot effectively compress the matrix to dewater it. In fact, the compressional strength of the GO-hematite microparticle matrix could be estimated from the applied force due to the magnetic field, although this would require a more carefully controlled magnetic field than was employed in the proof-of-principle measurements shown here. However, it is clear that the 'gel' matrix strength is on the same order as the force applied by the microparticles in the field, and that the nanoparticles and magnetic surfactants are insufficient to overcome the compressional strength of the GO matrix.

In contrast to previous studies where magnetic particles were found to have no significant compaction effect on dewatering of suspensions,[53] the fairly significant compression seen for

the GO-microparticle case indicates that for the loosely focculated 'gels' produced, magnetic compression is a viable and effective method for dewatering that merits further exploration.

pH reversibility of GO/hematite systems

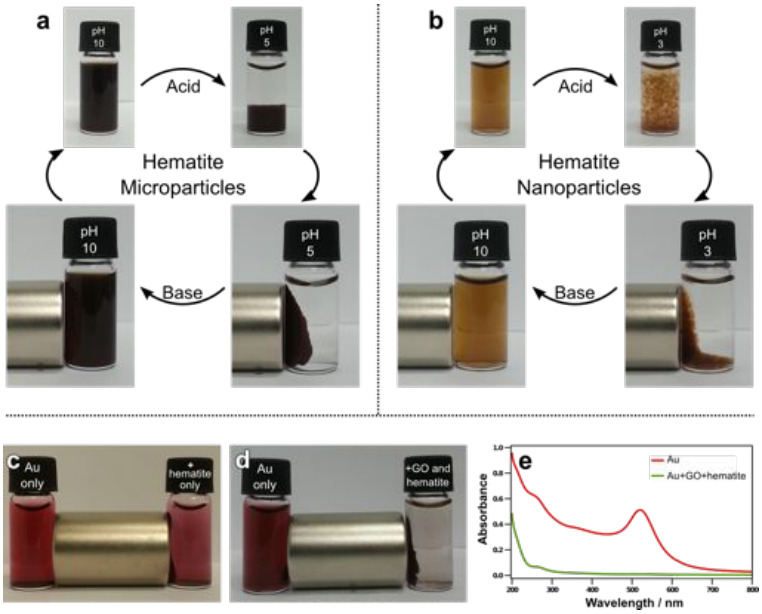

Figure 9: (a & b) Demonstrations of how system pH can be used to reversibly capture and redisperse GO in the presence of hematite microparticles (a) and hematite nanoparticles (b). (c) ~~The magnetic extraction of~~ At pH 3, hematite microparticles alone are unable to capture gold nanoparticles from ~~solution using~~ dispersion. Both vials contain the ~~GO/~~same concentration of gold nanoparticles, however the right-hand vial also includes 10 mg of hematite~~system~~. (d) A mixture of hematite microparticles and GO can effectively capture and extract gold nanoparticles from dispersion. Both vials contain the same ~~amount~~ concentration of gold nanoparticles, however the right-hand vial also includes 0.2 mg/mL of GO and 10 mg of hematite. (d) A UV-visible spectrum showing amount of gold present in the sample before and after capture with a magnet.~~The flat, green line corresponds to the supernatant solution of a sample containing ×10 the amount of GO and hematite as that represented by the purple line.~~

Having demonstrated that low pH conditions facilitate strong adsorption of hematite onto GO, it is pertinent to explore whether this process is reversible. The motivation is that if the captured material can be redispersed effectively, then GO can be used as a recyclable

adsorbent for (waste) water treatment. The ability to reuse the adsorbent multiple times offers clear energy, cost and environmental benefits. Figures 9a and 9b indicate that GO can indeed be reversibly captured with hematite microparticles or nanoparticles by changing the pH of the system. Acidic conditions facilitate the adsorption and capture of the GO, whereas readjusting the pH of the samples to moderately basic conditions serves to release the GO, restabilizing the dispersion and allowing selective separation of the magnetic particles from the GO.

These observations also serve to again indicate that surface charge is the overriding, driving force of the adsorption and dispersion processes for these materials, and van der Waals forces (expected to be comparatively weak for the single-layer GO) are of secondary importance. The approach of using non-covalent, charge based attractions in forming magnetic GO materials has significant advantages over existing magnetic GO composites, because in our case, the GO and the magnetic material are able to be recovered without any compromises to their original properties and hence, can be recycled or reused multiple times.

As a final demonstration of the power of this reversible deployment and capture process, we use the magnetic GO colloids to capture gold nanoparticles of diameter 10 nm from dispersion (Fig. ~~9c~~9d). By adjusting the pH to 3, the gold surface charge is moderately positive[54] and thus experiences an attractive electrical double-layer force for the GO surfaces which are negatively charged at this pH. The gold is expected to stick selectively to the GO surfaces, as the hematite is strongly positively charged at this pH. Fig. ~~9c–~~9e demonstrates conclusively from the loss of the characteristic plasmon signature for the gold particles that after application of the GO-hematite material and magnetic recovery of the matrix, the gold has been entirely removed from dispersion (at least within the detection limits of our experiment). The 'blank' experiment where only hematite particles are used, shown in Fig. 9c, demosntrates that GO is essential to this process, as the hematite and gold nanoparticles

are both positively charged at this pH.[54] This serves as a demonstration that non-covalent GO-hematite composite materials can be effectively deployed for adsorption and subsequent removal of nanomaterials from dispersion, with obvious applications in water treatment and nanomaterials processing.

Conclusion

The formation of non-covalent, magnetic graphene oxide (GO) materials was explored using three magnetic materials: hematite microparticles, hematite nanoparticles and magnetic surfactants. Each was found to co-flocculate GO at acidic pH, resulting in materials that could be captured using an external magnetic field. The adsorption of GO at low pH is attributed to attractive electrical double-layer forces between the GO and hematite or surfactants. Conversely in basic conditions, the dispersions remain stable due to like-charge repulsions, and it was shown that this provided a mechanism for the redispersion and separation of GO post-magnetic capture. Such non-covalent materials show obvious cost and energy benefits compared to bespoke syntheses of modified magnetic GO.[16–19]

The use of the magnetic surfactants and hematite nanoparticles minimizes the amount of adsorbate required for recovering GO, but are much less magneto-responsive when compared to hematite microparticles, which form a network with the GO that is not only captured, but also readily compressed by exposure to an external magnetic field. This magnetic dewatering result is more effective than for mineral systems,[53] and points to tempting methods for the further study of GO network properties and their compressional rheology.

An interesting effect was found with hematite nanoparticles, whereby low concentrations resulted in flocculation of GO and higher concentrations caused restabilization, most likely by

an effective over-charging of the GO surfaces. Such behaviour is not without precedent,[46,47] but has not been noted for carbon nanomaterials before, and provides a unique route to dispersions with enhanced stability and properties.

As well as magnetic capture of GO itself, these systems were shown to be effective for the removal of a model nanomaterial, gold nanoparticles, from water. These results demonstrate that the unique surface charging behaviour of aqueous GO systems can be readily exploited and manipulated to reversibly control the assembly of GO with various magnetic materials. By highlighting viable and recyclable colloidal techniques for deploying and removing GO from water, the need to create high energy and chemically complex covalent magnetic GO composites[17,19] is overcome, making its use in large scale water treatment more cost-effective and practical.

Materials & methods

Materials

Hematite (iron (III) oxide, Fe_2O_3), iron (II) sulphate heptahydrate, iron (II) dichloride tetrahydrate, phosphoric, sulfuric, and hydrochloric acids, potassium hydroxide and potassium permanganate (all 99% or greater) were obtained from ChemSupply and used without further purification. Hematite microparticles were prepared by grinding sintered hematite pieces (2-10 mm) in a pestle and mortar. The resulting powder was characterised using light microscopy and powder X-ray diffraction measurements. Hydrogen peroxide solution and aqueous ammonia (30% and 28% w/w in water respectively) were also from ChemSupply and used as received. Sodium tetrachloroaurate and sodium citrate were from Sigma. The magnetic surfactants 1-decyl-3-methyl imidazolium tetrachloroferrate (mim) and dodecyltrimethylammonium trichloromonobromoferrate (DTA) were synthesised and purified as described previously [25] . Mica disks used as substrates for AFM imaging were from ProSciTech (Thuringowa, QLD, Australia) and were freshly cleaved before use.

GO was synthesized from graphite flakes (Sigma, +100 mesh) from Bruceland (Clayton, Australia) using a variation on the Hummers method described in Marcano *et al.* [27] . The graphite powder (1 g) was dispersed

in 113 mL of a 9:1 ratio of concentrated sulphuric and phosphoric acids. This mixture was then stirred while potassium permanganate (6 g) was added gradually. The temperature was elevated to 50 °C and the reaction was left to stir overnight. The resultant orange/brown mixture was then left to cool to room temperature, and poured over ice (*ca.* 300 mL) with approximately 1 mL 30% H_2O_2. Large particles were removed from the crude reaction mixture by filtration, and the filtrate was then centrifuged at 6000 rpm for 1 hr and the supernatant liquid was discarded and replaced with distilled water. This process was repeated several times and the clean GO obtained was then dried at 45 °C.

Hematite nanoparticles were prepared from iron (II) sulphate heptahydrate (green vitriol) following the procedure of Chen *et al.* [45] . Iron (II) sulphate heptahydrate (8.36 g) was dissolved in 300 mL of water to create a 0.1 M solution. The addition of 30% w/w hydrogen peroxide solution (10 mL) rendered the mixture an intense orange colour, and this was then heated to 80 °C. In a separate vessel, 50 mL of aqueous ammonia (2.8% w/w) was heated to 60 °C, and then mixed rapidly with the orange iron solution. The mixture was allowed to stir for 20 minutes before the reddish precipitate was collected and washed five times by centrifugation and redispersion in ultrapure water. A small volume of iron (II) dichloride solution (0.6 mL, 0.1 M) was added to the washed suspension as a catalyst, and the solution was adjusted to pH 4 using hydrochloric acid and heated to boiling for 5 hours under reflux and gentle stirring. Upon completion of the reaction, gentle centrifugation (1000 rpm, 2 minutes) was used to remove any large particles, leaving a dark red solution of hematite nanoparticles.

Gold nanoparticles were synthesised using the method of McFarland *et al.* [55] . Briefly, a 1 mM solution of sodium tetrachloroaurate was heated to boiling with vigorous stirring, and to this, sodium citrate solution (38 mM) was added. The mixture was left to boil under stirring until the solution turned a deep red colour, indicating the presence of nanoparticles, after which the solution was allowed to cool.

Methods

Samples shown throughout were made up to a standard volume of 1.5 mL. Hematite was ground with a mortar and pestle before use, and pH adjustments were made with either hydrochloric acid or potassium hydroxide, and measured with a calibrated pH meter. Prior to analysis, all samples were equilibrated for at least 24 hours unless otherwise stated.

Magnetic response was assessed by placing a strong, permanent magnet beside or underneath the vials con-

taining the samples. The magnets used were composed of sintered NdFeB (M35) in a 100 μm thick nickel casing (Jaycar Electronics, Springvale, VIC, Australia). They were cylindrical in shape with diameter 19 mm and length 28.2 mm, and the magnetic field intensity at the surface was *ca* 1.2 T.

Magnetization data were collected for dried samples, which were placed in sealed polypropylene tubes and mounted inside a plastic straw for measurements in a magnetometer equipped with a superconducting quantum interference device (SQUID, MPMS XL, Quantum Design, San Diego, CA, USA).

UV-visible spectrophotometry measurements were carried out using a Cary 60 instrument from Agilent Technologies. The supernatant of each sample was analysed across a 200 - 800 nm wavelength range in clean, quartz cuvettes. For samples in which the concentration of surfactant was the point of interest, the GO was centrifuged down to ensure that the spectra obtained were representative of free surfactant only. Correspondence of the measured absorbance values to prepared calibration curves for GO and both magnetic surfactants were performed to obtain the post-adsorption concentrations of each material (see Supporting Information).

Dynamic light scattering measurements of hematite nanoparticles were made using a Brookhaven ZetaPlus instrument. The autocorrelation function of light scattered by the sample from a 30 mW red diode laser was fitted to obtain particle diffusion coefficients, D, and translated into apparent particle hydrodynamic radii, R_h, using the Stokes-Einstein equation.

Atomic force microscopy (AFM) imaging was performed using a JPK Nanowizard 3 AFM in AC (intermittent contact) mode using Bruker NCHV model cantilevers, which had nominal resonant frequencies of 340 kHz and spring constants of 20-80 N/m. Images were obtained with a set-point force of <1 nN and 'flattened' only by subtraction of a straight line from each scan line.

Supporting information available

Additional data on characterisation of GO, hematite and magnetic surfactant systems. This material is available free of charge via the Internet at http://pubs.acs.org.

References

1. Loh, K. P.; Bao, Q.; Eda, G.; Chhowalla, M. Graphene oxide as a chemical tunable platform for optical applications. *Nature Chem.* **2010**, *2*, 1015–1024.

2. Kim, J.; Cote, L. J.; Kim, W., F. Yuan; Shull, K. R.; Huang, J. Graphene Oxide Sheets at Interfaces. *J. Am. Chem. Soc.* **2010**, *132*, 8180–8186.

3. Kim, F.; Cote, L. J.; Huang, J. Graphene Oxide: Surface Activity and Two-Dimensional Assembly. *Adv. Mater.* **2010**, *22*, 1954–1958.

4. Kyzas, G. Z.; Deliyanni, E. A.; Matis, K. A. Graphene oxide and its application as an adsorbent for wastewater treatment. *J. Chem. Technol. Biotechnol.* **2014**, *89*, 196–205.

5. Chowdhury, I.; Duch, M. C.; Mandsukhani, N. D.; Hersam, M. C.; Bouchard, D. Colloidal Properties and Stability of Graphene Oxide Nanomaterials in the Aquatic Environment. *Environ. Sci. Technol.* **2013**, *47*, 6288–6296.

6. Konkena, B.; Vasudevan, S. Understanding Aqueous Dispersibility of Graphene Oxide and Reduced Graphene Oxide through pKa Measurements. *J. Phys. Chem. Lett.* **2012**, *3*, 867–872.

7. Li, D.; Muller, M. B.; Gilje, S.; Kaner, R. B.; Wallace, G. G. Processable Aqueous Dispersions of Graphene Oxide Nanosheets. *Nat. Nanotechnol.* **2008**, *3*, 101–105.

8. Gao, Y.; Li, Y.; Zhang, L.; Huang, G.; Hu, J.; Shah, S. M.; Su, X. Adsorption and removal of tetracycline antibiotics from aqueous solution by graphene oxide. *J. Colloid Interface Sci.* **2012**, *368*, 540–546.

9. Zhao, G.; Li, J.; Ren, X.; Chen, C.; Wang, X. Few-Layered Graphene Oxide Nanosheets As Super Sorbents for Heavy Metal Ion Pollution Management. *Environ. Sci. Technol.* **2011**, *45*, 10454–10462.

10. Yuan, Y.; Zhang, G.; Li, Y.; Zhang, G.; Zhang, F.; Fan, X. Poly(amidoamine) modified graphene oxide as an efficient adsorbent for heavy metal ions. *Polym. Chem.* **2013**, *4*, 2164–2167.

11. Babel, S.; Kurniawan, T. A. Low-cost adsorbents for heavy metals uptake from contaminated water: a review. *J. Hazard. Mater.* **2003**, *97*, 219–243.

12. Kemp, K. C.; Seema, H.; Saleh, M.; Le, N. H.; Mahesh, K.; Chandra, V.; Kim, K. S. Environmental applications using graphene composites: water remediation and gas adsorption. *Nanoscale* **2013**, *5*, 3149–3171.

13. Petit, C.; Bandosz, T. J. Synthesis, Characterization, and Ammonia Adsorption Properties of Mesoporous Metal-Organic Framework (MIL(Fe))-Graphite Oxide Composites: Exploring the Limits of Materials Fabrication. *Adv. Funct. Mater.* **2011**, *21*, 2108–2117.

14. Seredych, M.; Bandosz, T. J. Reactive adsorption of hydrogen sulfide on graphite oxide/$Zr(OH)_4$ composites. *Chem. Eng. J.* **2011**, *166*, 1032–1038.

15. Xu, C.; Cui, A.; Xu, Y.; Fu, X. Graphene oxide-TiO_2 composite filtration membranes and their potential application for water purification. *Carbon* **2013**, *62*, 465–471.

16. Zhang, K.; Dwivedi, V.; Chi, C.; Wu, J. Graphene oxide/ferric hydroxide composites for efficient arsenate removal from drinking water. *J. Hazard. Mater.* **2010**, *182*, 162–168.

17. Chandra, V.; Park, J.; Chun, Y.; Lee, J. W.; Hwang, I.-C.; Kim, K. S. Water-Dispersible Magnetite-Reduced Graphene Oxide Composites for Arsenic Removal. *ACS Nano* **2010**, *4*, 3979–3986.

18. Deng, J.-H.; Zhang, X.-R.; Zeng, G.-M.; Gong, J.-L.; Niu, Q.-Y.; Liang, J. Simultaneous removal of Cd(II) and ionic dyes from aqueous solution using magnetic graphene oxide nanocomposite as an adsorbent. *Chem. Eng. J.* **2013**, *226*, 189–200.

19. Fu, Y.; Wang, J.; Liu, Q.; Zeng, H. Water-dispersible magnetic nanoparticle-graphene oxide composites for selenium removal. *Carbon* **2014**, *77*, 710–721.

20. Sreeprasad, T. S.; Maliyekkal, S. M.; Lisha, K. P.; Pradeep, T. Reduced graphene oxide-metal/metal oxide composites: Facile synthesis and application in water purification. *J. Hazard. Mater.* **2011**, *186*, 921–931.

21. Das, M. R.; Borah, J. M.; Kunz, W.; Ninham, B. W.; Mahiuddin, S. Ion specificity of the zeta potential of a-alumina, and of the adsorption of p-hydroxybenzoate at the a-alumina-water interface. *J. Colloid Interface Sci.* **2010**, *344*, 482–491.

22. Teja, A. S.; Koh, P.-Y. Synthesis, properties, and applications of magnetic iron oxide nanoparticles. *Prog. Cryst. Growth Charact. Mater.* **2009**, *55*, 22–45.

23. Plaza, R. C.; Gonzalez-Caballero, F.; Delgado, A. V. Electrical surface charge and potential of hematite/yttrium core-shell colloidal particles. *Coll. Poly. Sci.* **2001**, *279*, 1206–1211.

24. Palomino, D.; Stoll, S. Fulvic acids concentration and pH influence on the stability of hematite nanoparticles in aquatic systems. *J. Nanopart. Res.* **2013**, *15*, 1428/1–8.

25. Brown, P.; Bushmelev, A.; Butts, C. P.; Cheng, J.; Eastoe, J.; Grillo, I.; Heenan, R. K.; Schmidt, A. M. Magnetic Control over Liquid Surface Properties with Responsive Surfactants. *Angew. Chem.* **2012**, *124*, 2464–2466.

26. Chen, J.-T.; Fu, Y.-J.; An, Q.-F.; Lo, S.-C.; Huang, S.-H.; Hung, W.-S.; Hu, C.-C.; Lee, K.-R.; Lai, J.-Y. Tuning Nanostructure of Graphene Oxide/Polyelectrolyte LbL Assemblies by Controlling pH of GO Suspension to Fabricate Transparent and Super Gas Barrier Films. *Nanoscale* **2013**, *5*, 1–7.

27. Marcano, D. C.; Kosynkin, D. V.; Berlin, J. M.; Sinitskii, A.; Sun, Z.; Slesarev, A.; Alemany, L. B.; Lu, W.; Tour, J. M. Improved Synthesis of Graphene Oxide. *ACS Nano* **2010**, *4*, 4806–4814.

28. Stankovich, S.; Dikin, D. A.; Piner, R. D.; Kohlhaas, K. A.; Kleinhammes, A.; Jia, Y.; Wu, Y.; Nguyen, S. T.; Ruoff, R. S. Synthesis of graphene based nanosheets via chemical reduction of exfoliated graphite oxide. *Carbon* **2007**, *45*, 1558–1565.

29. Cote, L. J.; Kim, F.; Huang, J. Langmuir-Blodgett Assembly of Graphite Oxide Single Layers. *J. Am. Chem. Soc.* **2009**, *131*, 1043–1049.

30. McCoy, T. M.; Pottage, M. J.; Tabor, R. F. Graphene Oxide-Stabilized Oil-in-Water Emulsions: pH-Controlled Dispersion and Flocculation. *J. Phys. Chem. C* **2014**, *118*, 4529–4535.

31. Lai, Q.; Zhu, S.; Luo, X.; Zuo, M.; Huang, S. Ultraviolet-visible spectroscopy of graphene oxides. *AIP Advances* **2012**, *2*, 1–5.

32. Moriya, T. Anisotropic Superexchange Interaction and Weak Ferromagnetism. *Phys. Rev.* **1960**, *120*, 91–98.

33. Dzyaloshinsky, I. A thermodynamic theory of 'weak' ferromagnetism of antiferromagnetics. *J. Phys. Chem. Solids* **1958**, *4*, 241–255.

34. Darab, M. I.; Shivashankar, S. A. Single crystalline magnetite, maghemite, and hematite nanoparticles with rich coercivity. *RSC Adv.* **2014**, *4*, 4105–4113.

35. Kovtyukhova, N. I.; Ollivier, P. J.; Martin, B. R.; Mallouk, T. E.; Chizhik, S. A.; Buzaneva, E. V.; Gorchinskiy, A. D. Layer-by-Layer Assembly of Ultrathin Composite Films from Micron-Sized Graphite Oxide Sheets and Polycations. *Chem. Mater.* **1999**, *11*, 771–778.

36. Zhao, X.; Zhang, Q.; Hao, Y.; Li, Y.; Fang, Y.; Chen, D. Alternate Multilayer Films of Poly(vinyl alcohol) and Exfoliated Graphene Oxide Fabricated via a Facial Layer-by-Layer Assembly. *Macromolecules* **2010**, *43*, 9411–9416.

37. Cassagneau, T.; Fendler, J. H. Preparation and Layer-by-Layer Self-Assembly of Silver Nanoparticles Capped by Graphite Oxide Nanosheets. *J. Phys. Chem. B* **1999**, *103*, 1789–1793.

38. Jang, J.-H.; Dempsey, B. A.; Burgos, W. A. Solubility of Hematite Revisited: Effects of Hydration. *Environ. Sci. Technol.* **2007**, *41*, 7303–7308.

39. Petzold, G.; Nebel, A.; Buchhammer, H.-M.; Lunkwitz, K. Preparation and characterization of different polyelectrolyte complexes and their application as flocculants. *Coll. Poly. Sci.* **1998**, *276*, 125–130.

40. Beresford-Smith, B.; Chan, D. Y. C. Electrical Double-layer Interactions in Concentrated Colloidal Systems. *Faraday Discuss. Chem. Soc.* **1983**, *76*, 65–75.

41. Beresford-Smith, B.; Chan, D. Y. C.; Mitchell, D. J. The Electrostatic Interaction in Colloidal Systems with Low Added Electrolyte. *J. Colloid Interface Sci.* **1985**, *105*, 216–234.

42. Chan, D. Y. C. Density functional theory of charged colloidal systems. *Phys. Rev. E: Stat., Nonlinear, Soft Matter Phys.* **2001**, *63*, 061806/1–8.

43. Carrique, F.; Arroyo, F. J.; Delgado, A. V. Electrokinetics of Concentrated Suspensions of Spherical Colloidal Particles with Surface Conductance, Arbitrary Zeta Potential, and Double-Layer Thickness in Static Electric Fields. *J. Colloid Interface Sci.* **2002**, *252*, 126–137.

44. Shih, C.-J.; Lin, S.; Sharma, R.; Strano, M. S.; Blankschtein, D. Understanding the pH-Dependent Behavior of Graphene Oxide Aqueous Solutions: A Comparative Experimental and Molecular Dynamics Simulation Study. *Langmuir* **2012**, *28*, 235–241.

45. Chen, X.-Q.; Wu, S.-B.; Cao, R.-B.; Tao, J.-S. Preparation and Characterization of Nanosized Hematite Colloids Using Green Vitriol as Ferrum Source. *J. Nanomater.* **2014**, 749562/1–8.

46. Herman, D.; Walz, J. Y. Stabilization of Weakly Charged Microparticles Using Highly Charged Nanoparticles. *Langmuir* **2013**, *29*, 5982–5994.

47. Ahualli, S.; Iglesias, G. R.; Wachter, W.; Dulle, M.; Glatter, O. Adsorption of anionic and cationic surfactants on anionic colloids: Supercharging and destabilization. *Langmuir* **2011**, *27*, 9182–9192.

48. Brown, P.; Butts, C. P.; Cheng, J.; Eastoe, J.; Russel, C. A.; Smith, G. N. Magnetic emulsions with responsive surfactants. *Soft Matter* **2012**, *8*, 7545–7546.

49. Brown, P.; Bushmelev, A.; Butts, C. P.; Eloi, J.-C.; Grillo, I.; Baker, P. J.; Schmidt, A. M.; Eastoe, J. Properties of New Magnetic Surfactants. *Langmuir* **2013**, *29*, 3246–3251.

50. Brown, P.; Khan, A. M.; Armstrong, J. P. K.; Perriman, A. W.; Butts, C. P.; Eastoe, J. Magnetizing DNA and Proteins Using Responsive Surfactants. *Advanced Materials* **2012**, *24*, 6244–6247.

51. Smith, G. N.; Eastoe, J. Magnetically-responsive electrophoretic silica organosols. *J. Colloid Interface Sci.* **2014**, *426*, 252–255.

52. Kletetschka, G.; Wasilewski, P. J.; Taylor, P. T. Hematite vs. magnetite as the signature for planetary magnetic anomalies? *Phys. Earth Planet. Inter.* **2000**, *119*, 259–267.

53. Watson, J. L.; Gardner, P. L. Multi-force dewatering for magnetic waste materials. *Minerals Eng.* **1995**, *8*, 191–200.

54. Tabor, R. F.; Morfa, A. J.; Grieser, F.; Chan, D. Y. C.; Dagastine, R. R. The Effect of Gold Oxide in Measurements of Colloidal Forces. *Langmuir* **2011**, *27*, 6026–6030.

55. McFarland, A. D.; Haynes, C. L.; Mirkin, C. A.; Van Duyne, R. P.; Godwin, H. A. Color My Nanoworld. *J. Chem. Educ.* **2004**, *81*, 544A–544B.

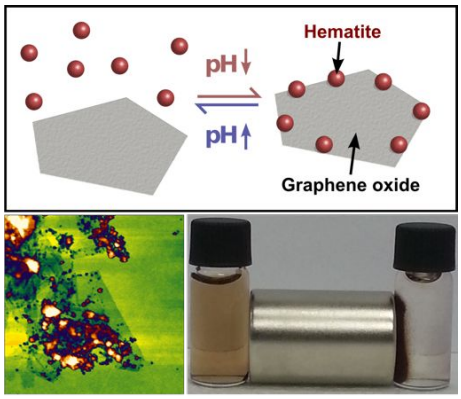

Figure 10: TOC graphic